Zhong and Gross *Journal of the European Optical Society-Rapid Publications* (2016) 12:3
DOI 10.1186/s41476-016-0004-x

Journal of the European Optical Society-Rapid Publications

RESEARCH Open Access

Phase space of partially coherent light with discontinuous surfaces

Minyi Zhong[1*] and Herbert Gross[1,2]

Abstract

We propagate partially coherent light through discontinuous surfaces and analyze the optical effects in phase space. The discontinuous surfaces are classified into two types, those with discontinuity in space and those with discontinuity in slope. Results are discussed based on the Wigner function. This approach explains the performance of segmented elements during the transition from the refractive into the diffractive regime. At first the diffraction effects generated by a single discontinuity (*e.g.* a phase step and a linear axicon) are investigated. Later on we discuss surfaces with periodic discontinuities, *e.g.* gratings, to study the formation of multiple diffracted orders. A kinoform lens is given as a further example to visualize the change from pure refraction to diffraction. Moreover, we present the beam homogenizing effect in phase space generated by lens arrays.

Keywords: Wigner function, Segmented element, Diffraction, Refraction, Interference

Background

The Wigner function was first proposed by Wigner [1] in 1932 as a quasi-probability distribution to describe quantum mechanics in phase space. Later the Wigner function was introduced into optics by Dolin and Walther [2–4], to describe an optical signal in phase space. There are several remarkable advantages of using the Wigner function for analyzing optical systems. First, it describes optical signals simultaneously in spatial frequency and space. This idea resembles the concepts of angle and position in geometrical optics. Making use of this property we are able to propagate light in phase space with the ray transfer matrix (also known as ABCD matrix) [5, 6]. Second, phase space visualizes information in wave optics such as diffraction and interference effects. Here we use the Wigner function as a tool to investigate segmented elements during the transition between refraction and diffraction. Third, the Wigner function is able to represent a partially coherent beam in a straightforward way [7]. It visualizes the degree of coherence in phase space as the angular extent. An alternative method to analyze partial coherence is to decompose a beam into a summation of modes [8, 9]. However, it requires a convergent mode expansion dependent on each specific problem. By using the Wigner function we avoid performing such complicated mode decomposition.

In this work we focus on light beams of spatial partial coherence, and propagate the beam through discontinuous surfaces. The optical effects are discussed in phase space. The content of this paper is divided into the following sections. Section 2 gives a brief introduction to the Wigner function. Section 3 discusses the diffraction effects generated by various discontinuous surfaces. We separate the discontinuous surfaces into two types, those with discontinuity in space, and those with discontinuity in slope.

Methods

We limit the discussions to two dimensions spatially, *i.e.* in coordinates (x, z) where x denotes the transverse position and z is the propagation direction. The light is restricted to be monochromatic, paraxial and partially coherent in space. Provided we know the cross-spectral density function $\Gamma(x_1, x_2)$ (also known as correlation function) of a partially-coherent beam at a certain transverse plane, where x_1 and x_2 are two arbitrary transverse coordinates, the phase space of light at this transverse plane is given by the Wigner function,

* Correspondence: minyi.zhong@uni-jena.de
[1]Friedrich-Schiller-University Jena, Institute of Applied Physics, Jena 07743, Germany
Full list of author information is available at the end of the article

$$W(x,u) = \int \Gamma\left(x+\frac{\Delta x}{2}, x-\frac{\Delta x}{2}\right)\exp\left(-i\frac{2\pi}{\lambda}u\Delta x\right)d\Delta x \tag{1}$$

where $x = (x_1 + x_2)/2$, $\Delta x = x_1 - x_2$. By definition, the integration of all signals in the Wigner function over the spatial dimension results in an angular spectrum. Integration of all the signals over the angular dimension computes the light intensity in space.

Figure 1 serves as an example to demonstrate the propagation of light inside a system by using Wigner functions. Inside the paraxial regions that can be described by ABCD matrices (*e.g.* z_1-z_6) we use Eq. 2 to propagate the Wigner function,

$$W'\left(x', u'\right) = W(Ax + Bu, Cx + Du) \tag{2}$$

where W and W' denote the Wigner functions of light entering and exiting a region respectively. In other regions consisting of lenses or stops (*e.g.* d_1-d_4), it is more convenient to obtain the correlation function Γ behind the element by a Fourier transform of the Wigner function, then employ the thin element approximation (Eq. 3–5). In this approach the thicknesses d_1- d_4 of the elements are neglected.

$$\begin{aligned}\Gamma'(x_1, x_2) &= \Gamma(x_1, x_2)\cdot t(x_1)\cdot t^*(x_2) \text{ or } (x_1, x_2)\\ &= \Gamma(x_1, x_2)\cdot A(x_1)\cdot A^*(x_2)\end{aligned} \tag{3}$$

$$t(x) = \exp\left[-i\frac{2\pi}{\lambda}(n\text{-}1)\Delta z(x)\right] \tag{4}$$

$$A(x) = \begin{cases} 1, & \text{inside stop} \\ 0, & \text{outside stop} \end{cases} \tag{5}$$

In Eq. 3–5 Γ and Γ' represent the correlation functions of light entering and exiting the region, t and A referring to the modulation functions for phase and for amplitude from a surface, λ being the wavelength, n being the refractive index of the element and Δz defining the height of the surface.

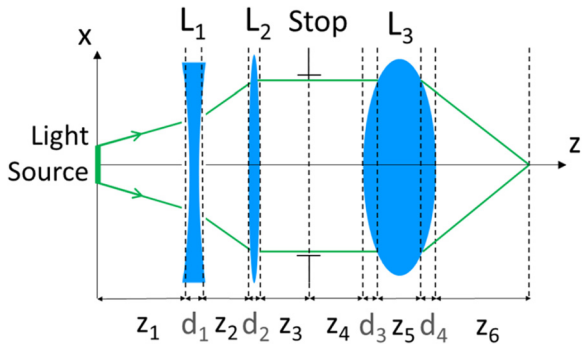

Fig. 1 Using the Wigner functions to propagate partially coherent light inside a system

Because of the Hermitian properties of the correlation function, the Wigner function is always in real but not necessarily positive values. Negative values in the phase space indicate destructive interference [10]. In the following section we discuss the interpretation of diffraction effects in phase space with various examples.

Results and Discussion

At first we introduce an important parameter Δφ to denote the optical path difference generated by a phase step (Fig. 2c). A ray of light in the wavelength λ traveling through a refractive material with a height of Δz accumulates the phase term $\exp(i2\pi n\Delta z/\lambda)$, where n is the refractive index of the material. Meanwhile another ray of light next to the material traveling through air of the same thickness Δz carries another phase term $\exp(i2\pi\Delta z/\lambda)$. We define the normalized phase difference between the two different rays as $\Delta\varphi = (n\text{-}1)\Delta z/\lambda$, i.e. the phase difference divided by 2π. In the special blazed condition, Δφ is an integer. It means the optical path difference is of a multiple of the wavelength. Thus it results in no interference effects. In the following discussions we concentrate on cases of Δφ being a non-integer to examine the diffraction effects.

Phase step

In this work the incident light source has a nearly flat-top transverse intensity profile, to insure a uniform illumination on the diffractive element. It is a superposition of multiple quasi-collimated monochromatic Gaussian Schell-model beams in the far field [11]. The source is characterized by three near-field parameters according to Eq. 12 in [11]: rms beam width σ, rms correlation width δ and the mode count M. The degree of coherence in our model decreases, when the value of σ increases. A larger integer of M produces a more flat-top profile of the far-field intensity.

We define the refractive index $n = 2.0$ for all optical elements and the wavelength $\lambda = 0.6328$ μm. In Fig. 2 the step heights are defined as $\Delta z = 50.0\lambda$, 50.2λ, 50.5λ, 50.8λ and 51.0λ, yielding $\Delta\varphi = 50.0$, 50.2, 50.5, 50.8 and 51.0 respectively (Fig. 2d-g).

With $\Delta\varphi = 50.0$ or $\Delta\varphi = 51.0$ there is no change in the phase space between the incoming beam and the outgoing beam (compare Fig. 2a, d). That is because the light experiences no phase jump after passing the step.

In the cases of Δφ being a non-integer (Fig. 2e-g), ripples occur in phase space. They are the visualization of diffraction effects centered at the step location. These diffraction ripples are an indication of the Fourier series of the Heaviside step function. In the case of $\Delta\varphi = 50.5$ the diffraction ripples are most pronounced and symmetric about the origin. In the intensity along the propagated

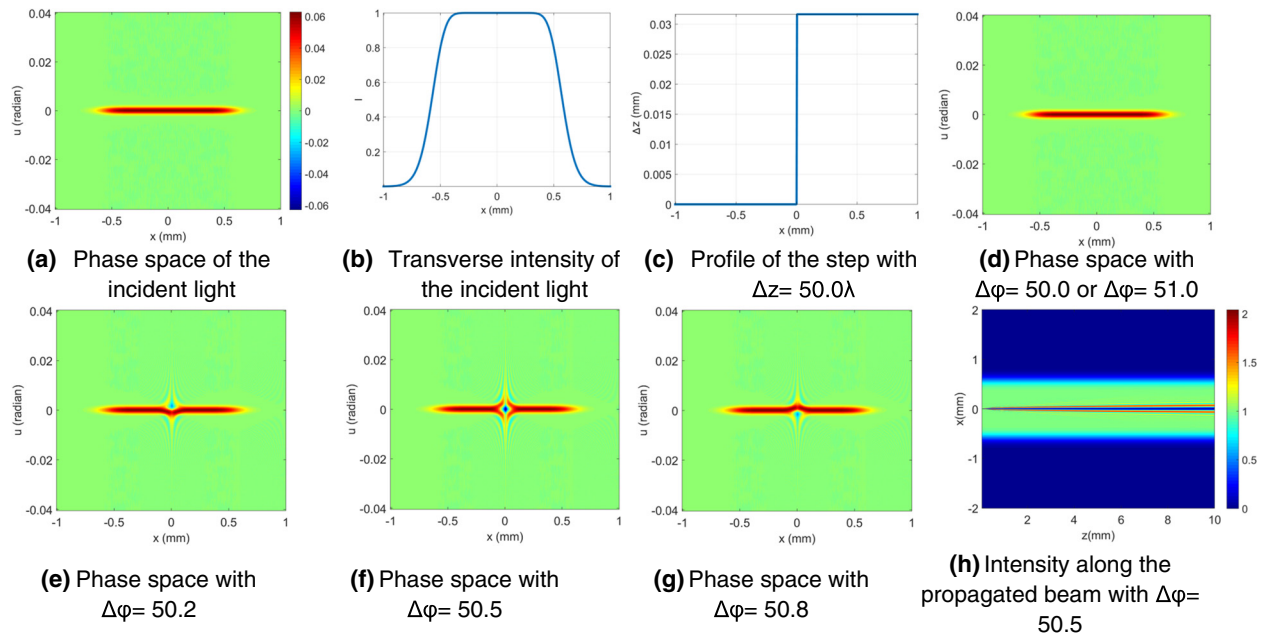

Fig. 2 Phase steps of various heights. The parameters for the incident light source are σ = 1 μm, δ = 0.5 μm and M = 40

beam (Fig. 2h) the destructive interference produces a minimum at the transverse intensity at x = 0. Besides, the phase space of Δφ = 50.2 (Fig. 2e) is a 180° rotation of the phase space of Δφ = 50.8 (Fig. 2g). The same applies to pairs of Δφ = 50.3 and 50.7, Δφ = 50.2 and 50.8, Δφ = 50.1 and 50.9.

It is worth mentioning that when the light source has a larger coherence length, the diffraction ripples are more pronounced. This is because a more coherent beam generates more noticeable interference effects. Conversely, as the coherence length of the light source decreases, the diffraction ripples become fainter.

Axicon

We take a linear axicon as another example to discuss the single discontinuity in phase. Compared to the phase step, a linear axicon is continuous in space but discontinuous in slope. Diffraction effects always happen when there is a slope discontinuity on the surface, even though there is no abrupt change for the step height. In this case Δφ is no longer a criterion to evaluate the destructive interference.

Corresponding results are shown in Fig. 3. The axicon splits a quasi-collimated incident beam (Fig. 3a) into two beamlets with different angles. This is indicated in the phase space (Fig. 3d) as two horizontal lines located at opposite angles. A split happens where the surface slope changes, *i.e.* x = 0.

In addition, diffraction ripples appear due to the phase wedge of the axicon. The ripples in Fig. 3d (i) and (ii) are connected to the two lines. They resemble the diffraction ripples generated by the phase step in Section 3.1. These ripples propagate with the beamlets and produce oscillations in the transverse intensity near the outer edges of the beamlets (Fig. 3g).

Meanwhile the ripples in Fig. 3d (iii) near the origin are separate from the two lines. They result from interference between the two beamlets. The ripple frequency increases with the angle between the two beamlets [12]. When we integrate these ripples over the angular axes, they produce oscillations in the transverse intensity. For a longer propagated distance, the ripples are sheared and their effect on the transverse intensity diminishes. The axial range where oscillations can still be observed (z < 3 mm) in the transverse intensity is proportional to the coherence length of the incident beam.

Grating

In the following we show several examples of phase space corresponding to various phase gratings.

A binary grating can be considered as a periodic superposition of Heaviside steps. The phase space of a single Heaviside step is discussed in the previous section (Fig. 2d-g). Here we start with a grating composed of four Heaviside steps. The grating profile is overlaid on top of the phase space in Fig. 4b. On the line with u = 0 in phase space, negative values occur at four separate x positions. These positions coincide with the phase discontinuity of the surface. Another notable feature in Fig. 4b is the positive peaks on the line through u = 0.033 radian. The three horizontal lines of signals along u = 0 and u = ±0.03 radian form the 0 and ±1 diffracted orders, respectively. The angles of diffracted orders follow the formula sin u = mλ/d, where u is the diffracted angle, m being the diffracted

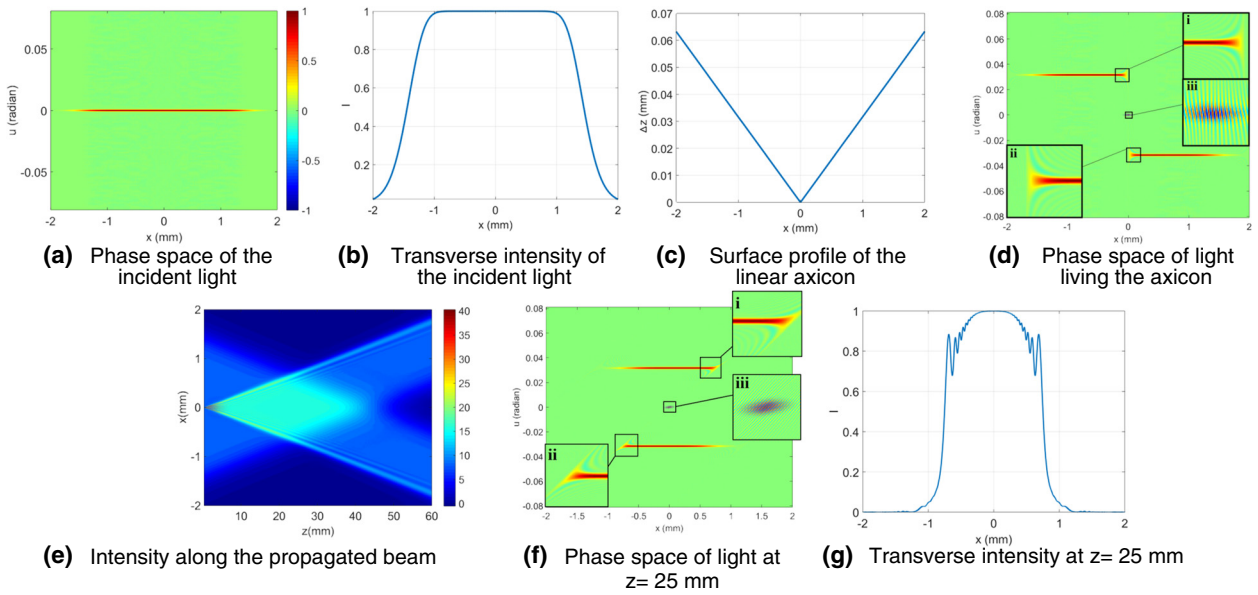

Fig. 3 Phase space of a quasi-collimated Schell-model beam passing a linear axicon. The parameters for the incident light source are $\sigma = 0.5$ μm, $\delta = 0.2$ μm and $M = 40$

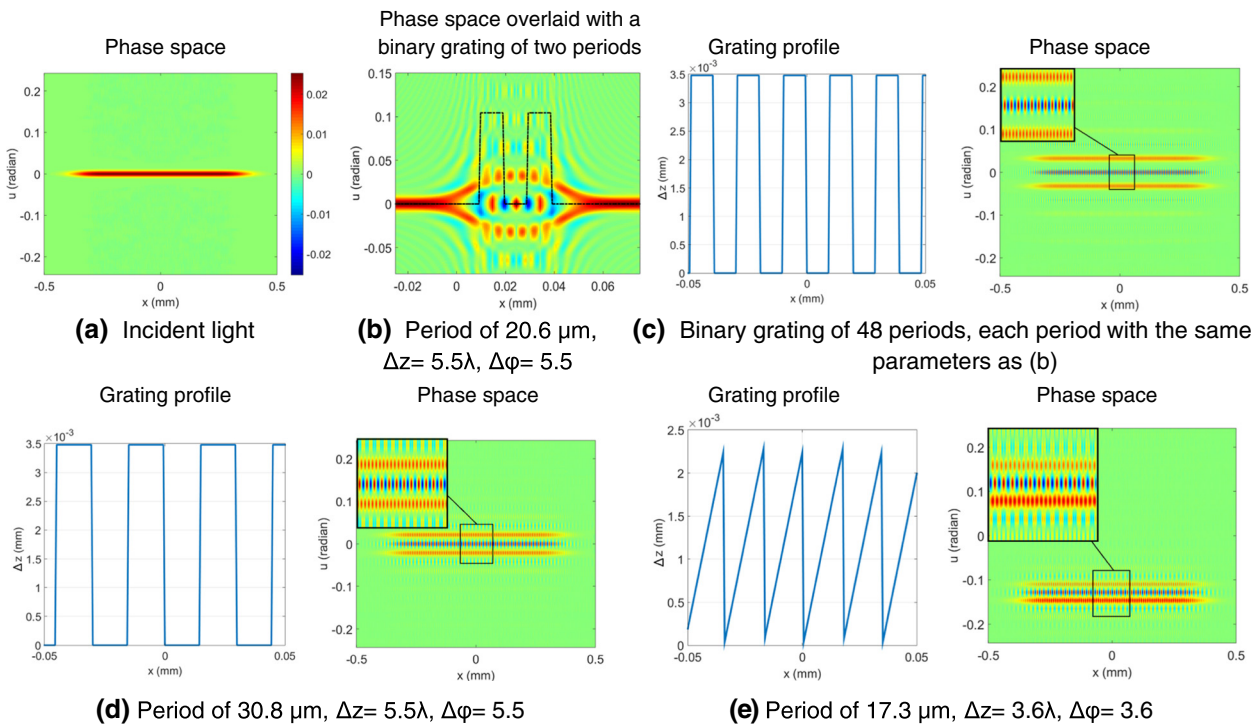

Fig. 4 Phase gratings. The total spatial extent of the gratings in (**c**), (**d**) and (**e**) is from −0.5 mm to 0.5 mm along the x axis. We only show the grating profiles along the x axis from −0.05 mm to 0.05 mm for a clear visibility of the periods. The parameters for the incident light source are $\sigma = 5$ μm, $\delta = 0.8$ μm and $M = 40$

order, λ representing the wavelength and d denoting the grating period.

In Fig. 4c the grating has the same period as the one in Fig. 4b, but covering a larger spatial extent. If we derive the angular spectrum from the phase space, there are sharper peaks representing the diffracted orders (not shown in the figures). However, the width of the peaks in the angular spectrum is also influenced by the angular extent of the partially coherent source. Figure 4d shows a binary grating with a larger period. According to the diffraction formula, a larger value of d results in a smaller diffracted angle u. The ±1 diffracted orders are at u = ±0.023 radian. Figure 4e illustrates a blazed grating (also called echelette grating). Due to the asymmetric profile of this grating, both refraction and diffraction take place. All the diffracted orders move along the angular axis. The 0 order is repositioned at the angle u = −0.12 radian.

Moreover, the step height of the blazed grating defines the value of the normalized phase difference Δφ. With Δφ = 3.6, the −1 order contains more energy than the +1 order (Fig. 4e). For a binary grating, the energies in the +1 and −1 orders are always equal.

Kinoform lens

A kinoform lens can be interpreted as a grating with locally varying periods. When the periods can be approximated by a linear blazed grating, one may use the method proposed by Sinzinger [13] to analyze the diffraction effects based on Fourier analysis. In our work we express the profile of the kinoform lens as a conical surface with $z = cx^2/\{1 + [1-(1 + k)c^2x^2]^{1/2}\}$, where c denotes the curvature (*i.e.* the reciprocal of the radius) and k is the conic constant. We cut this surface into slices with an equal height Δz, and leave out all the coplanar parts. This cutting yields a kinoform lens with quadratically-decreasing zone widths from the inner to the outer region (Fig. 5a). The profiles of individual grooves remain conical. We discuss the

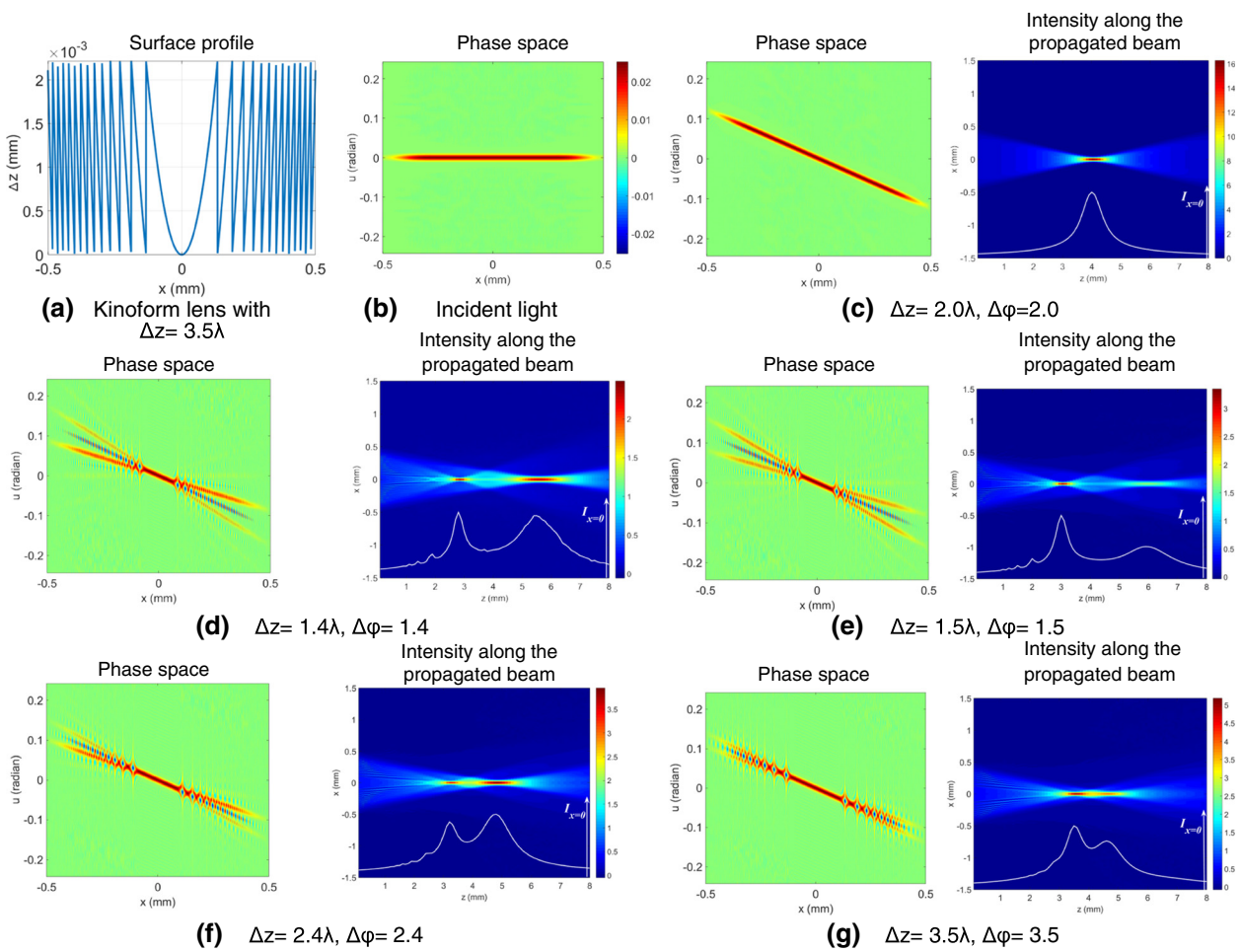

Fig. 5 Kinoform lenses with various groove heights. The lens profile in (**a**) does not have perfectly uniform groove heights due to finite samplings. The zone widths vary from 10.4 to 41.8 μm in (**c**), from 7.8 to 34.6 μm in (**d**), from 7.8 to 36.6 μm in (**e**), from 11.7 to 47 μm in (**f**), and from 17.6 to 55.4 μm in (**g**). Figures of phase space share the color bar in (**b**). The parameters for the incident light source are σ = 5 μm, δ = 0.7 μm and M = 40

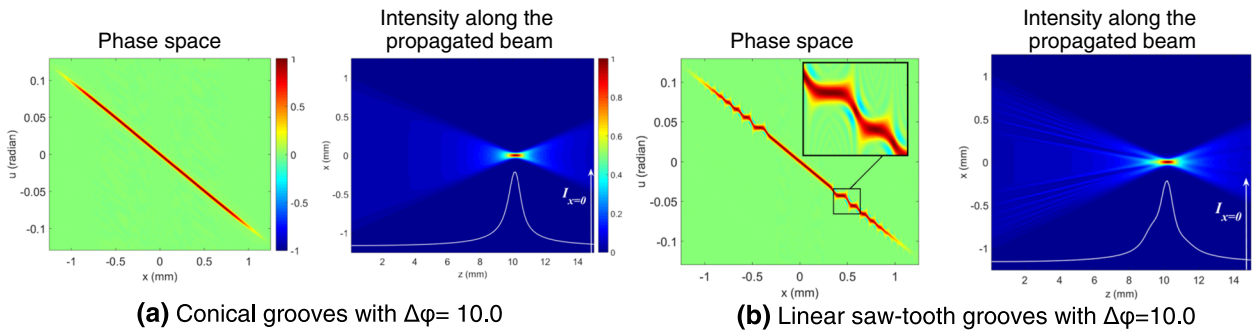

Fig. 6 Fresnel lens with conical grooves (**a**) and linear saw-tooth grooves (**b**), both with a focal length of 10 mm. Figures with the same titles share the same color bars. The parameters for the incident light source are σ = 2 μm, δ = 0.3 μm and M = 40

diffraction effects generated by such a kinoform lens in Fig. 5, with c = 0.25 mm^{-1}, k = −4 and various values of Δz.

When the kinoform lens works in blazed condition we call it a Fresnel lens (Fig. 5c, Δφ = 2.0). In this case the transmitted light is dominated by refraction. Ray optics is sufficient to describe its optical effects in the paraxial regime. In phase space the focusing effect of the Fresnel lens is expressed by a shearing of signals along the angular axis. The propagation of light is performed by an additional shearing along the spatial axis. At the focus position the signals in phase space form a vertical line. As there are no diffraction ripples in phase space, the intensity along the propagated beam is symmetric about the focal plane (z = 4 mm).

When the kinoform lens does not fulfill the blazed condition, *i.e.* Δφ being a non-integer, the phase mismatch generated by the groove height can contribute to significant diffractive phenomena. Multiple diffracted orders appear when the zone widths on the kinoform lens are in the range of several wavelengths.

In Fig. 5c the phase space is composed of several stripes crossing each other at the origin. Each stripe represents one diffracted order. The central stripe is the 0 order indicating the refracted beam path. Thus the 0 order is always at the same location as the phase space signals in Fig. 5b. Any other higher orders (±1, ±2, *etc.*) are the outcomes of interference effects. The fine structures in phase space result from a superposition of all the interference effects generated by individual grooves.

With Δφ between 1.4 and 2.4 the diffracted orders are separated from each other by a large distance. In free-space propagation, each diffracted order produces its own axial focus. The energy ratio of the foci depends on the energy distribution among the diffracted orders. With Δφ = 1.5, both +1 and −1 orders contain equal energy in phase space. Correspondingly the foci formed by the +1 and −1 orders share the same amount of energy. However, due to different numerical apertures, their peak heights are not equal. Meanwhile there is no intensity peak at z = 4 mm for Δφ = 1.5 in Fig. 5d. That is because the integration of the phase space signals i the 0 order returns zero.

The transition from diffraction to pure refraction happens when the zone width grows considerably larger than the wavelength (λ = 0.6328 μm). When the height of the kinoform lens is increased to Δz = 3.5λ, *i.e.* Δφ = 3.5, the zone width is above 17 μm. The diffracted orders are no longer distinguishable (Fig. 5f). All the diffracted orders start to merge together. Individual foci in the propagated

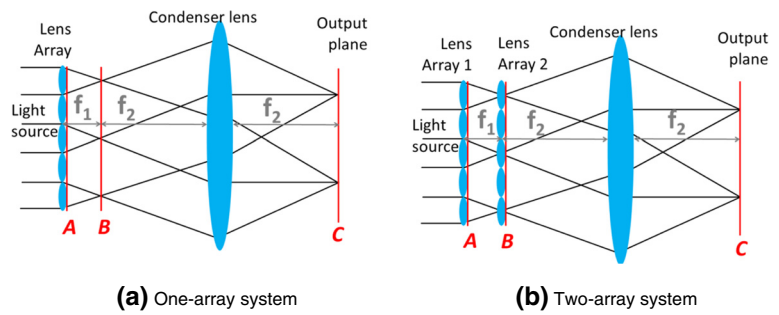

Fig. 7 Setups for beam homogenizing. The focal length of the lens array is f_1. The focal length of the condenser lens is f_2. Plane A marks the plane right behind the array. Plane B lies on the back focal plane of the array. Plane C is the output plane for a homogenized beam

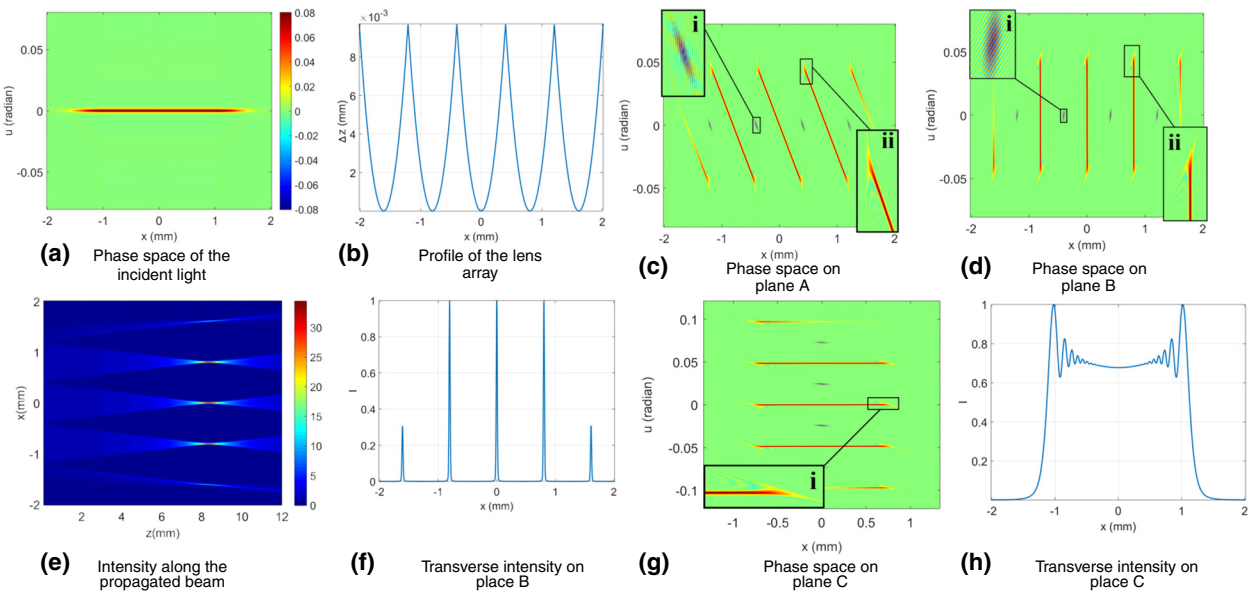

Fig. 8 Phase space results of the one-array system for beam homogenizing given by Fig. 7a. Figures of phase space share the color bar in (**a**). The parameters for the incident light source are σ = 1 μm, δ = 0.18 μm and M = 40

beam path are not separable any more. If the zone width is increased even more, diffraction effects gradually fade. Eventually this leads to one single focus as in ray optics.

Due to manufacturing limitations, a Fresnel lens is commonly produced with linear saw-tooth grooves. In Fig. 6 we compare this type of Fresnel lens ($\Delta\varphi = 10.0$) and a lens with conical grooves. Because $\Delta\varphi$ is an integer, the Fresnel lens with conical grooves gives exactly the same performance as a continuous conical lens. The axial intensity distribution along propagation is symmetric about the focus position (Fig. 6a). Correspondingly, a Fresnel lens with linear saw-tooth grooves is equivalent to a piecewise linear approximation of a conical surface. This approximation creates discontinuous slopes on the surface, although the groove height yields no phase mismatch due to $\Delta\varphi$ being an integer. The corresponding diffraction effects are seen in phase space as additional ripples. Furthermore, the linear profile on each groove bends the light into slightly non-focusing angles. Under the influence of ray effects and wave effects, an asymmetric axial focus is found in the propagated beam path (Fig. 6b).

Lens array

The lens array is a common component in optical systems for beam homogenizing. Figure 7 shows two setups for this application.

Figue 8 shows the results based on the setup in Fig. 7a. The light leaving the array is distributed into five channels defined by the individual lenslets. This is indicated by five parallel tilted lines in phase space on the plane A (Fig. 8c). Between the adjacent lines there are additional diffraction ripples caused by the discontinuous slope of the array.

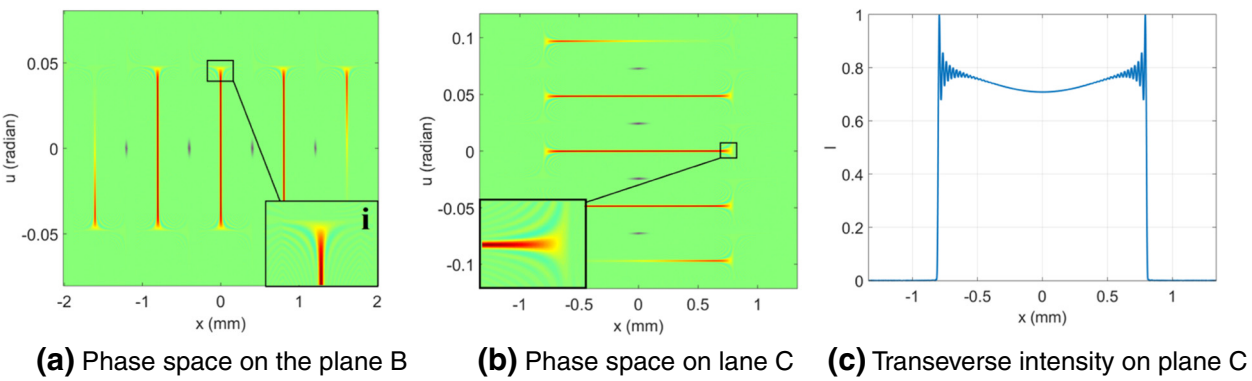

Fig. 9 Phase space results of the two-array system for beam homogenizing given by Fig. 7b. Phase space in (**a**) and (**b**) share the color bar in Fig. 8a

Similar to the case of an axicon, ripples occur near the zero angle regions and at each end of the five lines (Fig. 8c (i) and (ii)). As the plane B is at the back focal plane of the lens array, five tilted lines in phase space on the plane A are sheared into a vertical orientation (Fig. 8d). By integrating the signals in Fig. 8d vertically we derive five narrow peaks in the transverse intensity on the plane B (Fig. 8f). They indicate five focused beamlets at the back focal plane of the lens array. The weaker intensity peaks in Fig. 8f originate from the non-uniform illumination. The ripples in Fig. 8d (i) give no contribution to the transverse intensity after the integration.

Since the plane B and the output plane C form a pair of Fourier conjugates, the phase space on the plane C is a 90° rotation of the phase space on the plane B. The ripples in Fig. 8g (i) produce oscillations in the transverse intensity at the edges of the beam (Fig. 8h).

The only difference between the two setups in Fig. 7 is the second lens array. It is placed at the back focal plane of the first array, acting as a field lens. This field lens introduces an extra focusing effect. In phase space this is expressed as a vertical shearing of signals. Thus the ripples in Fig. 9a (i) are sheared into a symmetric distribution, compared with Fig. 8d. Physically it means the field lens captures light with large angles and bends them into the acceptable numerical aperture of the condenser lens. Thus the light falls into a better-defined spatial region on the output plane C. Figure 9c shows a more homogenized intensity profile than Fig. 8h.

Conclusions

The Wigner function contains information about ray optics and wave optics. In this work the Wigner function helps us to understand the behavior of partially coherent light interacting with diffractive elements. We discuss two types of discontinuous surfaces, those with discontinuity in space and those with discontinuity in slope.

The phase step, grating and kinoform lens belong to the first type. For surfaces of spatial discontinuity, the optical path difference is important to evaluate the destructive interference. For example, by varying this parameter we see the change of a kinoform lens from pure refraction to diffraction. This parameter also controls the energy distribution among the multiple foci formed by the diffracted orders of a kinoform lens.

The axicon, Fresnel lens with linear saw-tooth grooves and the lens array represent the second type of surface discontinuity, *i.e.* discontinuity in slope. It always causes pronounced interference effects.

The Wigner function is a useful tool for optical simulation. It facilitates the interpretation of intermediate optical effects, in particular for complex systems with partially coherent light and diffractive elements.

Competing interests
The authors declare that they have no competing interests.

Authors' contributions
Both authors developed the simulation models together. The progress is a result of common contributions and discussions. MZ implemented the work and wrote the manuscript. HG proposed the original ideas, gave advices and offered the conditions for the project. Both authors read and approved the final manuscript.

Acknowledgements
This work is partially supported by the German Federal Ministry of Education and Research within the project fo+ (03WKCK1D). We thank Dr. Martin Kielhorn for comments and discussions which improved this manuscript. We are grateful to the reviewer for the constructive input.

Author details
[1]Friedrich-Schiller-University Jena, Institute of Applied Physics, Jena 07743, Germany. [2]Fraunhofer Institute for Applied Optics and Precision Engineering IOF, Jena 07745, Germany.

Received: 3 April 2016 Accepted: 9 May 2016
Published online: 23 June 2016

References

1. Wigner, E: On the quantum correction for thermodynamic-equilibrium. Physical Rev **40**, 749–759 (1932)
2. Dolin, L: Beam description of weakly-inhomogeneous wave fields. Izv Vyssh Uchebn Zaved Radiofiz **7**, 559–563 (1964)
3. Walther, A: Radiometry and coherence. J Opt Soc Am **58**, 1256–1259 (1968)
4. Walther, A: Propagation of the generalized radiance through lenses. J Opt Soc Am **68**, 1606–1610 (1978)
5. Eppich, B: Die Charakterisierung von Strahlungsfeldern mit der Wigner-Verteilung und deren Messung. Doctoral dissertation, Technical University of Berlin, Germany (1998)
6. Testorf, M, Hennelly, B, Ojeda-Castaneda, J: Phase-Space Optics: Fundamentals and Applications. The McGraw-Hill companies, New York (2010)
7. Bastiaans, M: Application of the Wigner distribution function to partially coherent light. J Opt Soc Am A **3**, 1227–1238 (1986)
8. Wolf, E: New theory of partially coherence in space-frequency domain. Part I: Spectra and cross-spectra of steady-state sources. J Opt Soc Am **72**, 343–351 (1982)
9. Wolf, E: New theory of partial coherence in the space-frequency domain. Part II: Steady-state fields and higher-order correlations. J Opt Soc Am A **3**, 76–85 (1986)
10. Signer, W, Totzek, M, Gross, H: Handbook of Optical Systems-Physical Image Formation. Wiley-VCH, Weinheim (2005)
11. Korotkova, O: Random sources for rectangular far fields. Opt Lett **39**, 64–67 (2014)
12. Hlawatsch, F: Interference terms in the Wigner distribution. Digital Signal Processing. **84** 363–367 (1984)
13. Sinzinger, S, Testorf, M: Transition between diffractive and refractive micro-optical components. Appl Opt **34**, 5970–5976 (1995)